Experimental Determination of Maximum Effective Hydrodynamic Stress in Multiphase Flow Using Shear Sensitive Aggregates

Thomas K. Villiger, Massimo Morbidelli, and Miroslav Soos
Dept. of Chemistry and Applied Biosciences, Institute for Chemical and Bioengineering, ETH Zurich, 8093 Zurich, Switzerland

DOI 10.1002/aic.14753
Published online February 18, 2015 in Wiley Online Library (wileyonlinelibrary.com)

Maximum effective hydrodynamic stress, τ_{max}, responsible for the breakup of aggregates with size comparable to Kolmogorov eddies, was experimentally determined in an aerated stirred tank. The proposed method is based on the measurement of the maximum stable aggregates size consisting of poly(methyl methacrylate) nanoparticles. The fractal aggregates were broken under various operating conditions in an aerated stirred tank and calibrated with known flow conditions using contracting nozzles to convert the measured aggregate sizes into hydrodynamic stress. It was found that τ_{max} can vary substantially among studied conditions and its magnitude depends on the controlling mechanism including gas jet during bubble formation, bubble rise, bubble burst at the gas–liquid interface or the turbulence generated by the impeller. The measured values are in good agreement with literature data which supports the applicability of this method to characterize the maximum effective hydrodynamic stress in complicated multiphase flow. © 2015 American Institute of Chemical Engineers *AIChE J*, 61: 1735–1744, 2015

Keywords: aggregate breakage, stirred tank, maximum hydrodynamic stress, contracting nozzle, gas–liquid flow, bubble rise, bubble burst, gas jet velocity

Introduction

Both sparging and stirring are commonly applied in bioreactors during the cultivation of mammalian cells.[1,2] Although stirring is used to provide homogenization and mass transfer, sparging is crucial for oxygenation of the cultivation broth. Despite a large effort of researchers to study the effect of hydrodynamic stress on cell cultures,[1,3,4] no generally accepted method for hydrodynamic stress quantification in complex turbulent multiphase flows occurring during cell cultivation has been proposed.[1,5] The reason for the lack of an universal quantification method are multiple phenomena acting simultaneously, that is, stress generated by the gas jet occurring during bubble detachment from the sparger,[6] stress induced during bubble rise,[7] and burst,[8] or stress generated by the turbulent flow due to impeller motion.[9]

Although single-phase flow fields in stirred tanks equipped with various impellers have been characterized using different experimental techniques such as Laser-Doppler anemometry (LDA),[10,11] particle image velocimetry (PIV),[12,13] or constant temperature anemometry (CTA),[14–16] these techniques struggle with limitations regarding multiphase flow. In particular, the presence of bubbles disturbs the optical signal of LDA or changes the heat transfer of the fluid when CTA is used. To overcome these limitations, PIV systems using two cameras and fluorescent seeding particles have been developed.[17] While the first camera captures the scattered signal from the fluorescent particles dispersed in the liquid phase, the second camera monitors the scattered signal from bubbles which allows to measure both velocity components of the liquid and gas phase, respectively.[18–20] Most of the presented results are restricted for angle resolved and angle-averaged flow fields in the liquid and bubble phase as well as for the measurement of velocity fluctuations of both phases. A large-eddy PIV method was applied to compensate for low resolution of the PIV technique allowing an estimation of the turbulent dissipation rate.[21] Several other experimental techniques such as Positron Emission Particle Tracking (PEPT),[22] computer-automated radioactive particle tracking computer tomography (CARPT),[23–25] and multiwave ultrasound technique[26] have been used to characterize the local gas volume fraction in stirred tanks. However, due to their low spatial and temporal resolution they are not suitable to characterize the small scale turbulence structures including highest local ε values.

Alternative methods to determine maximum local energy dissipation rate or hydrodynamic stress are applying indirect characterization measurements using shear sensitive systems. Values of ε_{max} have been estimated by measuring the maximum stable droplet size,[27] the breakup kinetics of clay particles,[28,29] or using processes affected by the level of shear rate while measuring the mass transfer through the boundary layer.[30] These approaches do not provide any space

Correspondence concerning this article should be addressed to M. Soos at miroslav.soos@chem.ethz.ch.

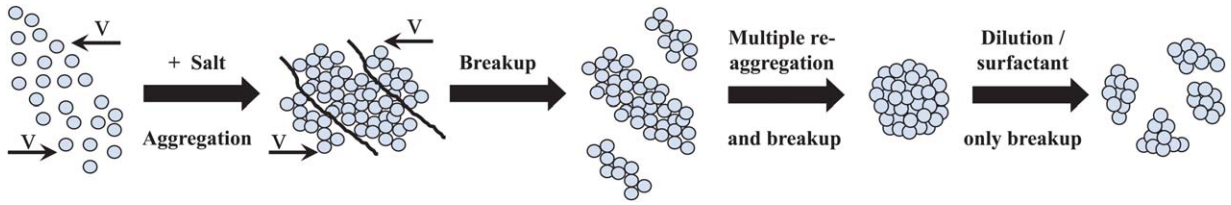

Figure 1. Schematic representation of aggregation and breakage experiments.

Salt-induced aggregation of primary particles under shear form large clusters which undergo multiple aggregation and breakage events until a steady-state cluster size is reached (round cluster). After dilution of the system, reaggregation is stopped and the maximum effective hydrodynamic stress becomes the controlling mechanism for the final aggregate size.

[Color figure can be viewed in the online issue, which is available at wileyonlinelibrary.com.]

information about the location or abundance of ε_{max} values. Nevertheless, they can be applied to identify corresponding maximum effective stresses at or close to real operating conditions including multiphase flows.

The main goal of this work is to characterize the maximum effective hydrodynamic stress, τ_{max}, in an aerated stirred tank from different sources including stress generated by the gas jet occurring during bubble detachment from the sparger, stress induced by rising and bursting bubbles, and stress generated by the turbulent flow due to impeller motion. The applied system uses shear sensitive aggregates which break immediately when exposed to a hydrodynamic stress exceeding their strength. After all aggregates have experienced the highest stress causing aggregate breakup, the steady-state aggregate size is measured and used to estimate the maximum effective hydrodynamic stress present in the system. As the size of steady-state aggregates is comparable to the size of Kolmogorov eddies, the maximum effective hydrodynamic stress refers to an average stress occurring on the length scale of smallest eddies. The occurrence of such stresses has to be frequent enough so that all aggregates experience the highest stress value at least once. Therefore, effects of rare events of very high stresses, caused by intermittency of the turbulent flow, are not covered by the presented method. In contrast to previous indirect methods, the steady-state aggregate size rather than kinetics of size reduction[31,32] is used for the determination of τ_{max}. In addition, the system can be applied in pure water or using a surfactant containing solution.

Materials and Methods

Methyl methacrylate (MMA), sodium dodecylsulphate (SDS), and potassium persulphate (KPS) used in poly(methyl methacrylate) (PMMA) nanoparticle synthesis were obtained from Acros Organics. Sodium chloride and Pluronic® F-68 was purchased from Sigma-Aldrich.

Primary nanoparticle synthesis

PMMA primary particles were prepared by monomer-starved semibatch emulsion polymerization.[33] After dissolving 0.1 g of SDS in 89.9 g deionized water under nitrogen atmosphere, the solution was heated up to 80°C using an external oil bath followed by an addition of 0.07 g of radical initiator (KPS). A programmable syringe pump (VIT-FIT LAMBDA, Switzerland) was used for the addition of 10 g methyl methacrylate (MMA) at a flow rate of 0.1 g/min. After MMA addition, the polymerization was continued for an additional 2 h to ensure complete monomer conversion. Dynamic light scattering measurement using a Zetasizer Nano (Malvern Insruments, UK) confirmed monodispersity of PMMA nanoparticles with a mean diameter equal to 62 nm.

Stirred tank geometry

Stirred tank experiments were performed in a flat bottom reactor with a tank diameter, T, equal to 160 mm. It was equipped with a Rushton turbine with diameter $D=3T/8$ located in $T/3$ from the vessel bottom and four rectangular baffles connected to the wall with a width equal to $T/10$ and a thickness of $T/80$. The liquid level was set equal to the tank diameter resulting in a working volume of 3.2 L. Various stirring speeds have been applied, ranging from 50 up to 700 rpm corresponding to impeller Reynolds numbers $Re_{imp}=\rho_L N D^2/\mu_L$ from 3×10^3 to 4.2×10^4, combined with air flow rates from 0 to 140 L/h. The gas inlet was placed in the middle between the vessel bottom and the impeller pointing toward the side wall of the vessel. The horizontal installation of the gas inlet allowed to investigate a broad range of gas flow rates including very high gas inlet velocities above 30 m/s which was documented to cause cell death.[6] An upward pointing gas inlet was inapplicable at that scale to keep the gas jet completely within the liquid phase. Different aeration nozzles having diameters of 0.4, 0.7, 1, 2, and 8 mm (wall thickness was always equal to 1 mm) in combination with various gas flow rates were used to generate gas jet velocities ranging from 0.08 up to 155 m/s which correspond to gas jet Reynolds numbers, $Re_{jet}=d_{nozzle}v_{air}\rho_{air}/\mu_{air}$, of 2.5×10^3 up to 7.1×10^4. A sinter sparger with an average pore diameter of 50 μm was installed to generate small bubbles. Pictures of single rising bubbles were taken with a Leica D-Lux 3 camera and analyzed using the MATLAB Image Processing Toolbox to estimate the distribution of the circle equivalent diameter and its mean Sauter diameter D_{32} (see Supporting Information Figure 1).

Aggregation and breakup experiments

In a typical breakage experiment, the initial suspension of PMMA nanoparticles was aggregated in a 2-L beaker with a latex mass fraction, ϕ, of 1×10^{-2}. A 0.2 mol/L sodium chloride solution, well above the critical coagulation concentration (CCC), and a 40-mm pitch blade impeller operated at 50 rpm were used for the initial aggregation of primary PMMA nanoparticles. At such high salt concentrations, no electrostatic repulsion exists between primary particles so that they hold together within an aggregate only by van der Waals forces.[34] After reaching a steady-state cluster size, which is controlled by a dynamic equilibrium between aggregation and breakage (see Figure 1),[35] the initial aggregates were gently withdrawn and diluted in the testing stirred tank filled with deionized water. The high dilution factor of

200 reduces the salt concentration to 1 mM and the final particle mass fraction to 5×10^{-5}, preventing any reaggregation as the final salt concentration is well below the CCC of the nanoparticles. The selected dilution was chosen not to exceed the maximum obscuration of 30% defined as a threshold value of the light scattering device.

As soon as the hydrodynamic stress exceeds the strength of the aggregates, they will break until a new steady-state size is reached.[36–38] Since the source of the maximum effective hydrodynamic stress can originate from rising bubbles which can also burst at the air–liquid interface,[8,39–41] surfactant (Pluronic® F-68) was optionally added to prevent the attachment of aggregates to rising bubbles.[42,43] Preliminary experiments using various surfactant concentrations confirmed that aggregates break easily at low surfactant concentration even in mild gassing conditions. Therefore, all experiments were either performed without surfactant or with a surfactant concentration equal to 0.5 g/L. The selected surfactant Pluronic® F-68 is commonly used as a protecting agent in cell cultures with comparable concentration to avoid cell attachment to the rising bubble and, therefore, minimize their presence during bubble burst.[40,44]

Once the steady-state cluster size was reached, an offline sample of 25 mL was gently withdrawn and measured by small angle light scattering (SALS), Mastersizer 2000 (Malvern Instruments, UK). Data analysis was performed following our previous works.[36,37,45–48] The mean radius of gyration, $\langle R_g \rangle$, was used to characterize the size of the aggregate clusters while the fractal dimension, d_f, was extracted from the power law region of the structure factor to depict their internal structure.

A short summary about the application of this technique is provided in Supporting Information. Once the steady state was characterized, the stirring speed or gas flow rate was increased and the procedure was repeated after reaching a new steady state. By starting from low and moving toward higher stress conditions, by either increasing stirring speed or gas flow rate, the entire range of both investigated parameters can be investigated using the same initial aggregates. To verify that the reduction of aggregate size was solely controlled by their breakup and not by any internal restructuring, the fractal dimension, d_f, was determined for all operating conditions. The uncertainty of determining $\langle R_g \rangle$ using SALS is in the order of 10% of its value.[35,46] The actual measured standard deviation of approximately 5% from experimental repetitions correspond to the size of the data points and are exemplary shown in Supporting Information Figure 2.

Relation between aggregate size and maximum effective stress

In isotropic turbulence, several flow types including extensional flow, rotation in eddies, shear flow, and streams coexist which transport the fluid from one point to another.[49] Although eddies and streams occupy most of the volume, they exert only small stress on particles or aggregates. In contrast, zones with extensional or simple shear flows occupy a rather small fraction of the volume with zones where highest stresses will be exerted on dispersed particles or aggregates.[38,50–52] As pointed out by several authors,[38,50,51] extensional flow is more efficient for aggregate breakup compared to simple shear. This is due to a permanent deformation which aggregate experience in extensional flow in contrast to an oscillatory deformation occurring in simple shear evolving from a rotation of the principle axis of the rate of strain with respect to the liquid flow direction.[37,53,54]

In the presence of bubbles in the liquid phase, several phenomena which could cause high stress values subsist and hence lead to aggregate breakup. Detailed numerical simulations of bursting bubbles[8] have shown that zones exposed to the highest stress are associated with an extensional flow located beneath the bursting bubble. A similar observation was found by Gordillo et al.[55] who investigated bubble formation and detachment from aeration nozzles. As a result of mass conservation within the fluid, a liquid jet with very high velocity impinging the bottom side of the bubble is formed. Due to the axial symmetry of the bubble, this local jet can be approximated by an extensional flow.[55]

The flow field around rising bubbles is more complex and strongly depends on the shape and size of the rising bubbles, as reported by several authors.[7,56,57] Although the flow around small spherical bubbles is laminar with the highest values of the stress located in the boundary layer on its surface, the increase of rising velocity measured for larger bubble size results in the formation of a pair of vortexes within the bubble wake.[56,57] By further increasing the bubble size, the wake becomes instable forming a von Karman vortex street[56] which together with a nonspherical shape of the bubbles leads to an unstable flow pattern behind the bubbles. The investigated bubble sizes in this work range from 1.5 to 10 mm which corresponds to bubble Reynolds numbers from 200 to 2000. Under these conditions, the flow in the von Karman vortex street behind a single rising bubble covers transient as well as turbulent conditions.[58] However, as shown by Koynov et al.[7] the presence of multiple bubbles with a Reynolds number of 75 result in an additional disturbance of the flow in the wakes. Therefore, assuming turbulent flow in the bubbles wakes under all conditions, the most probable mechanism for cluster breakup is caused again by extensional flow. It is worth noting that a steady simple shear flow in the bubble wakes would decrease the values of the hydrodynamic stress approximately by a factor of 2.[36,52,53]

Taking all aforementioned arguments into consideration, the relation between the steady-state aggregate size and the applied maximum hydrodynamic stress was constructed by breaking the initial aggregates in axisymmetric extensional flow generated at the entrance of contracting nozzles of various diameters and flow rates (see Table 1). Following an experimental procedure developed earlier,[36,37] the aggregate suspension was pumped several hundred times through the nozzle to guarantee complete breakage of all aggregates. The evolution of the clusters $\langle R_g \rangle$ was monitored by small-angle light scattering and summarized in Supporting Information. The steady-state aggregate size was correlated to the maximum hydrodynamic stress present in the contracting nozzle calculated from full three-dimensional time-dependent simulation of the Navier–Stokes equation.[36] As it was shown in our previous work,[9] using peak values of the corresponding hydrodynamic stress calculated in a contracting nozzle with those calculated in a stirred tank, the stable aggregate size measured in the both devices closely correlate independent whether the flow is laminar or turbulent.

The maximum effective hydrodynamic stress reported in this work is based on the following assumptions: as indicated by Soos et al.[9] the steady-state size of aggregates is comparable to the size of the smallest Kolmogorov eddies present

Table 1. Hydrodynamic Properties Calculated by CFD for Different Contracting Nozzles and Volumetric Flow Rates

d_{nozzle} (mm)	Q (mL/min)	Re_{nozzle}	$\langle\tau\rangle$ (Pa)	τ_{max} (Pa)
3.0	80	566	0.6	1.7
2.0	55	584	1.4	4.2
1.5	40	566	2.5	7.6
1.5	80	1132	5.4	16.2
1.0	55	1167	13.6	40.7
0.75	40	1132	24.7	74.0
0.75	80	2264	52.8	158.3

in the impeller vicinity. Under such conditions, the rate of single breakage event is proportional to the applied shear rate, which is inversely proportional to the Kolmogorov timescale.[59] The latter is under all investigated conditions in the range of milliseconds to microseconds. Conversely, the measurement of aggregates sizes by light scattering is realized on the assembly of many aggregates. Hence, the majority of the population, which consists in our case of approximately 10^7-10^{11} aggregates, has to go through many breakage events. Thus, the determined value of τ_{max} represents an ensemble as well as time averaged value over many breakup events on the level of Kolmogorov eddies rather than a single-local value.

Results and Discussion

Steady-state cluster size and cluster morphology

PMMA nanoparticles are stabilized by electrostatic repulsive forces preventing their aggregation. The addition of salt above the CCC results in a complete screening of these repulsive forces, and therefore, inducing polymer nanoparticles aggregation (see Figure 2). The clusters grow until the point where hydrodynamic stress exceeds the strength of the aggregates leading to aggregate breakage. Aggregate fragments can undergo reaggregation and subsequent breakup resulting in a dynamic equilibrium between aggregation and breakup characterized by a steady-state aggregate size.[35] This equilibrium can be disturbed by increasing stirring speed or changing the salt concentration which resulting in a new steady state. This is illustrated in Figure 3 where aggregates reduce their size after a change in salt concentration until a new steady state is reached (after 40–50 min). When approximating the time scale of a single breakage event by the Kolmogorov timescale, which was for this particular condition in the order of 10^{-4} s, few million breakage events per second are required to reach a steady state within 40 min. This is in agreement with previous discussions indicating that all aggregate have to experience highest stress values at least once to reach a steady-state aggregate size.[36,37,59] As the breakup of aggregates under turbulent conditions could be affected by the presence of intermittency,[27,60] special attention was dedicated to ensure that the steady state was reached under all conditions. No significant impact on the aggregate size or the aggregate structure was observed by increasing the time interval from 2 to 12 h. This indicates that the effect of intermittency on the studied process is negligible, at least within the timescale applied in this work, and the selected time period of 2 h is sufficient to ensure steady-state condition. Such a small effect of intermittency is in agreement with the theoretical work of Bäbler[61] which investigated the breakup of aggregates under turbulent conditions generated in a stirred tank with comparable power input. Based on these results, the steady-state aggregate size was measured 2 h after every change of operating condition.

Aggregates are fractal like objects and they could possibly undergo restructuring which would increase their compactness without any breakup events. Hence, it is important to ensure that there is no variation of the internal structure during breakup events. When evaluating d_f from the slope of the power law region of $S(q)$, it was found that all data follow the same scaling with d_f equal to 2.7 independent whether the aggregates were measured before or after dilution and consequent breakup (see Supporting Information Figure 3). Such a high value of d_f is in close agreement with our previous studies[36,38] confirming that shear-induced aggregation forms very compact clusters.

Aggregate size calibration

To characterize the maximum hydrodynamic stress in the studied stirred tank, the initial aggregates were first broken by well-defined extensional flows generated in contracting nozzles.[36,37] Hereafter, the dependency of the maximum

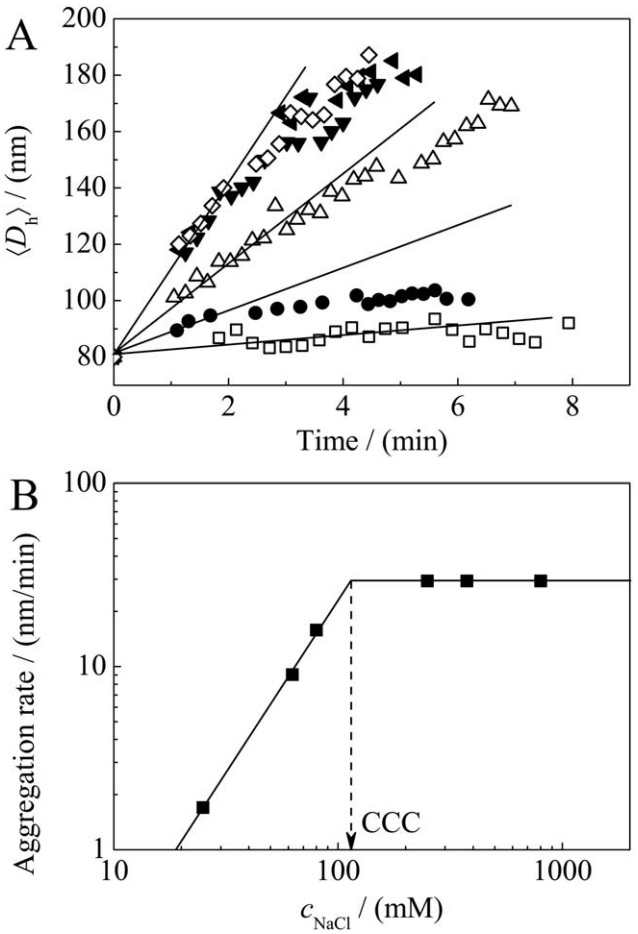

Figure 2. Initial PMMA nanoparticle aggregation rate at various salt concentrations.

(A) Average hydrodynamic diameter of aggregate clusters as a function of time measured under stagnant conditions: cNaCl = 25 mM (open squares), cNaCl = 62.5 mM (close circles), cNaCl = 80 mM (open up triangles), cNaCl = 250 mM (closed down triangles), cNaCl = 375 mM (open diamonds), cNaCl = 800 mM (closed left triangles). Lines show the initial aggregation rate. (B) Initial aggregation rates plotted as a function of salt concentration together with the definition of the critical coagulation concentration (CCC).

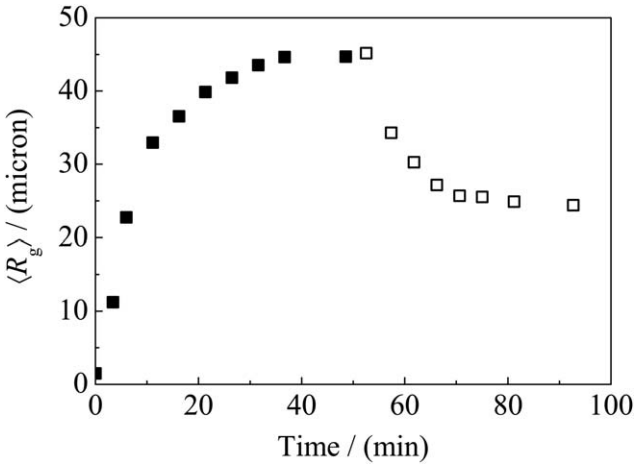

Figure 3. Illustration of a typical aggregation experiment to prepare initial aggregates and the effect of dilution on their size.

The system was diluted with a factor of 1:200 after reaching a dynamic equilibrium between aggregation and breakup. The salt concentration well below CCC prevents any reaggregation leading to a new steady state with smaller $\langle R_g \rangle$.

stable aggregate size as a function of known stress can be determined. Because the maximum stable aggregate size is independent whether the flow is laminar or turbulent with respect to the peak stress values,[9] the size of aggregates measured in a complex flow field can be used to estimate the corresponding maximum effective hydrodynamic stress.

An example of a breakage experiment using a contracting nozzle is presented in Figure 4A. The measured $\langle R_g \rangle$ is monotonically decreasing with the number of passes and several hundred passes are required until a steady-state size is reached. This slow decay is caused by a broad distribution of the hydrodynamic stress at the nozzle entrance where only a small fraction of aggregates is broken in the zone of highest stress during a single pass.[36,37] Therefore, the dispersion of aggregates was passed through the contracting nozzle 300 times before a steady-state aggregates size was characterized by light scattering. The decrease of $\langle R_g \rangle$ is solely controlled by the aggregate breakup as no change of d_f was observed in this case (see Supporting Information Figure 3). The scaling of $\langle R_g \rangle$ as a function of maximum hydrodynamic stress (see Table 1) is presented in Figure 4B, visualizing a decrease in cluster size with increasing hydrodynamic stress. The power law scaling with a slope equal to -0.74 is indicated by a solid line in Figure 4B. This is in good agreement with the theoretical scaling of -0.66 according to Zaccone et al.,[62] using d_f equal to 2.7, being equivalent to the experimentally measured value (see Supporting Information Figure 3). The power law scaling of $\langle R_g \rangle$ versus τ_{max} shown in Figure 4B was used to convert steady-state cluster sizes measured under various conditions in the stirred tank to the corresponding maximum effective hydrodynamic stress.

As it was shown in our previous study of aggregate breakup in a turbulent stirred tank,[9] the maximum stable size of aggregate fragments is comparable to the size of the Kolmogorov eddies. Under this condition, the aggregate breakup is controlled by the value of the hydrodynamic stress which is proportional to the properties of the fluid and the local value of the turbulent energy dissipation rate ε_{max} according to

$$\tau_{max} = \sqrt{\mu_L \rho_L \varepsilon_{max}} \quad (1)$$

where the dynamic viscosity, μ_L, and the density, ρ_L, of water at 25°C was used to relate the maximum effective hydrodynamic stress to ε_{max} present in the system. As mentioned above, the calculated ε_{max} represents an effective value required for the breakup of the studied aggregate clusters.

Higher gassing flow rates have been reported to form gas cavities and thus decrease the power number of Rushton impellers. However, the used sparger configuration pointing toward the side wall of the vessel generate a gas jet which circumvented the impeller at high gas flow rates. In this way, gas cavities behind the impeller blades were avoided[63] and no significant drop of the power number of the studied Rushton impeller could be observed (see Supporting Information Figure 4).

Effect of process conditions on aggregates size

Several phenomena occurring in gas–liquid systems such as gas jets,[6] bubble rise,[7] or bubble burst,[8,64] can be a source of high hydrodynamic stress. They are acting simultaneously under common cultivation conditions and even though one

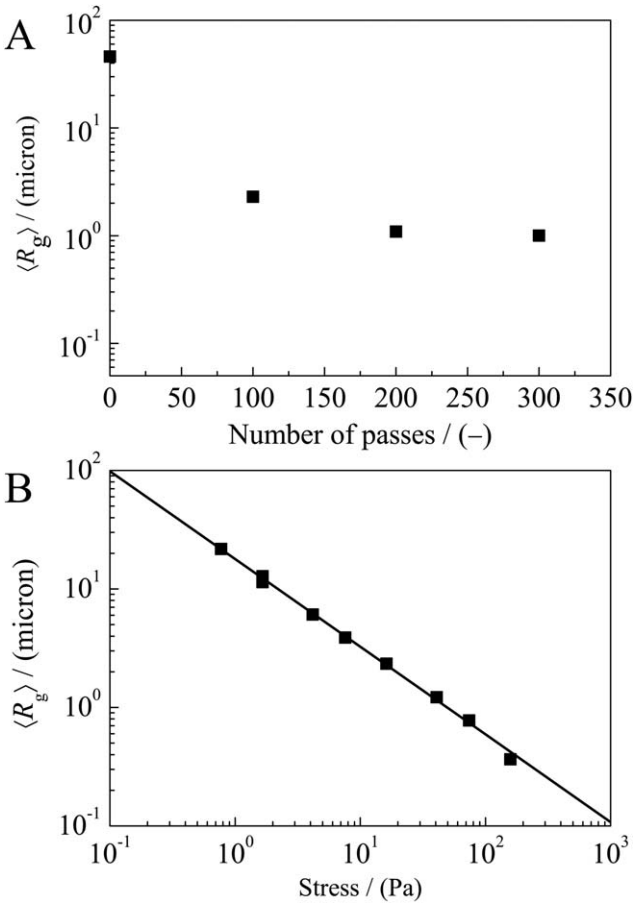

Figure 4. Aggregate breakup in contracting nozzles.

(A) Aggregate breakup as a function of passes through a contraction nozzle. (B) Steady-state $\langle R_g \rangle$ measured after 300 passes through the nozzle plotted as a function of the maximum effective hydrodynamic stress (see Table 1).

Table 2. Applied Operating Conditions for Figures 5, 6, and 8

Sparger Outlet (mm)	Gas Flow Rate (L/h)	D_{32} (mm)	Re_{jet}	Surfactant (g/L)	Symbol
–	–	–	–	0.5	Closed squares
–	–	–	–	0	Open squares
0.05	3	1.6	–	0	Closed up triangles
0.7	7	3.9	101	0	Open up triangles
0.05	3	1.3	–	0.5	Closed gray circles
0.7	7	4.0	101	0.5	Open circles
8	14	10.1	41	0.5	Closed circles
0.4	14	–	825	0.5	Open down triangles
1	140	–	3300	0.5	Closed down triangles

particular mechanism might be dominant, other operating parameters might influence the peak stress value. Therefore, operating parameters such as stirring speed, gas flow rate, bubble size, and the velocity of the gas jet formed at the gas inlet were increased until a particular mechanism was prevailing and thus different regimes could be identified. A summary of the applied conditions is presented in Table 2.

The measured cluster size decrease as a function Re_{imp} measured for single-phase conditions is presented in Figure 5A. This effect is independent whether surfactant was present in the system or not, clearly indicating that the dilution alone is sufficient to stop any further reaggregation of clusters with breakup being the only mechanism controlling their size. However, the presence of bubbles significantly affects the measured cluster size even at mild gassing conditions. In particular, the steady-state cluster size at low Re_{imp} is controlled by the size of the generated bubbles where smaller clusters $\langle R_g \rangle$ were measured for 1.6-mm bubbles compared to 5.9-mm bubbles (see Figure 5B). On increasing Re_{imp}, the cluster size becomes progressively more dependent on Re_{imp} until a critical point where the turbulence generated by the impeller takes over and the measured cluster size $\langle R_g \rangle$ is similar to that measured for single phase. The cluster breakup, and thus, also the steady-state cluster size, is controlled by the highest stress present in the system which is dominated by the interplay between turbulence generated by the impeller and the stress resulting from the presence of bubbles in the stirred tank. The observed sudden reduction of the $\langle R_g \rangle$ measured for 5.9-mm bubbles is related to their breakup occurring at $Re_{imp} > 10^4$ which generated small bubbles with comparable diameter to those introduced into the system by a 50-μm sinter sparger. Due to the hydrophobic nature of the PMMA particles, they will attach to gas bubbles in surfactant free conditions. The small size of cluster measured for surfactant free conditions indicate that the cluster attach to bubbles and are therefore exposed to high stress events at the gas–liquid interface such as bubble burst[1,8] even at mild gassing conditions. In fact, the measured aggregate concentration in the foam was comparable to the concentration in the liquid in surfactant free condition.

In contrast, the addition of surfactant prevents the attachment of aggregates to bubbles and consequently they will be not exposed to high stress values present during bubble burst.[1,8] The steady-state aggregate sizes, $\langle R_g \rangle$ plotted as a function of Re_{imp} measured for single- and two-phase conditions in the presence of surfactant are depicted in Figure 6. The cluster size measured at low Re_{imp} decreases with increasing bubble sizes from 1.3 to 10.1 mm. Interestingly, small bubbles generated by a 50-μm sinter sparger showed no significant impact on the measured cluster sizes when surfactant was present (gray circles in Figure 6A, which is a completely opposite trend compared to the small clusters measured in surfactant free conditions shown in Figure 5B). This indicates that two different mechanisms are responsible for aggregate breakup in surfactant free and surfactant containing conditions. The negligible amount of aggregates (below the detection limit of the light scattering device)

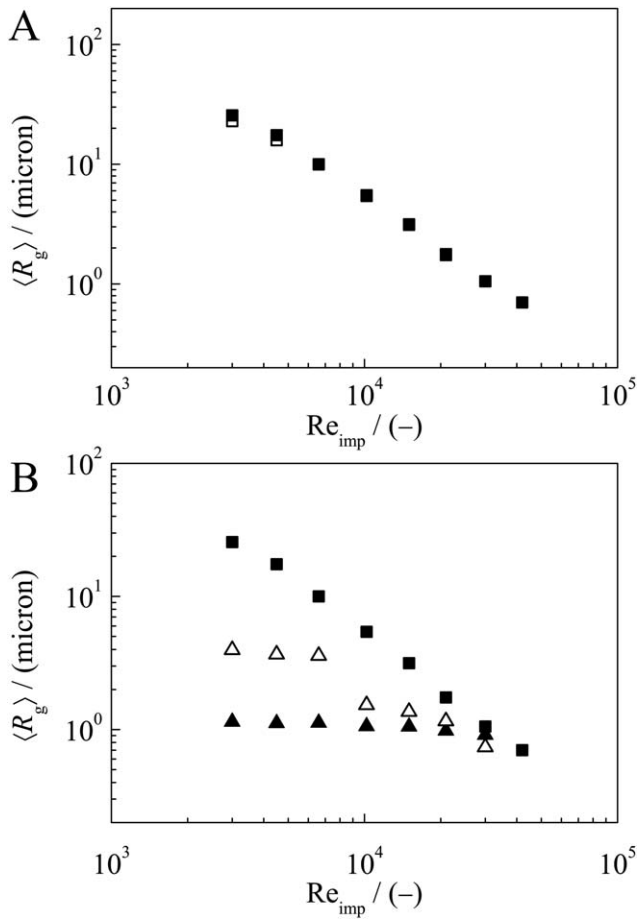

Figure 5. Radius of gyration as a function of impeller Reynolds number measured with and without surfactant.

(A) $\langle R_g \rangle$ as a function of Re_{imp} measured with 0.5 g/L surfactant (closed squares) and in surfactant free solution (open squares). (B) $\langle R_g \rangle$ as a function of Re_{imp} in surfactant free solution without sparging (closed squares), with aeration using a nozzle (open up triangles) and a sinter sparger (closed up triangles). The applied conditions are summarized in Table 2.

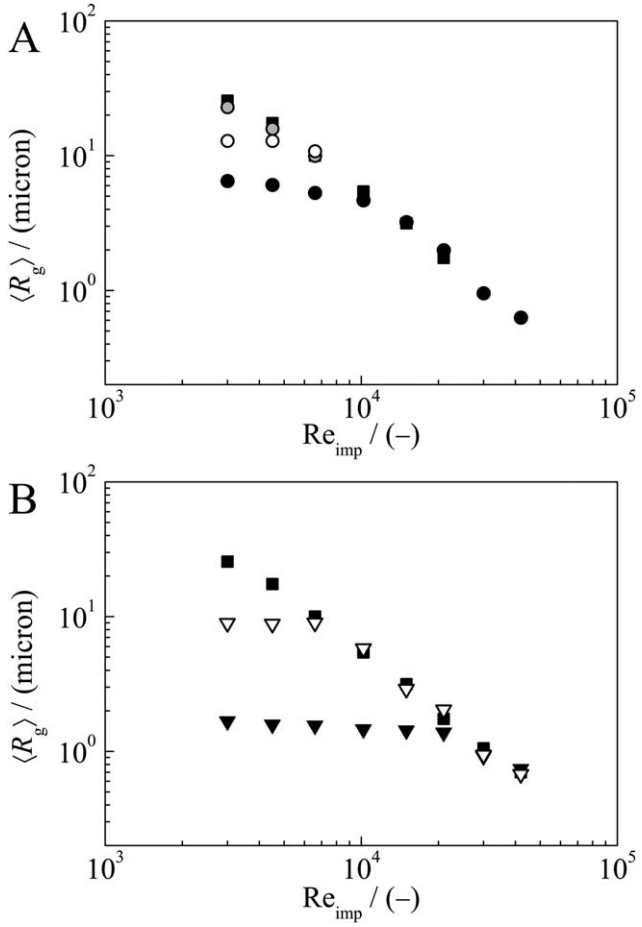

Figure 6. Radius of gyration as a function of impeller Reynolds number measured for single-phase and two-phase condition using 0.5 g/L surfactant.

(A) Effect of bubble size on the steady-state cluster size. (B) Effect of different Re_{jet} on steady-state cluster size. The applied conditions are summarized in Table 2.

measured in the foam when surfactant was present further supports the assumption of nonattaching aggregates in surfactant containing conditions.

It is worth noting that all aforementioned experiments were performed with jet Reynolds number, Re_{jet}, below 200 corresponding to gas inlet velocities below 1.2 m/s. As it was reported that high gas jet velocity could be detrimental for cell cultures,[6] the stress generated by different gas jet velocities was further studied by varying the gas flow rate and aeration nozzle diameter. To eliminate possible effects of bubble burst, all experiments with high Re_{jet} were collected in the presence of 0.5 g/L surfactant. Figure 6B shows the aggregate size at two different Re_{jet} of 165 and 3300 corresponding to the gas inlet velocities of 1.2 and 150 m/s, respectively. It can be seen that the aggregate size decreases substantially as Re_{jet} increases at low Re_{imp}. Similar to previous experiments, stirring becomes dominant after reaching a critical Re_{imp}, and the measured aggregate size is comparable to single phase conditions.

The consistency of the aggregates' internal structure for all conditions was verified by evaluating the fractal dimension, d_f, by plotting $S(q)$ as a function of $q\langle R_g \rangle$. As can be seen from Figure 7, d_f remains unchanged and equal to 2.7, independent whether the aggregates were broken in single- or two-phase flow, with or without surfactant. The change of aggregate sizes is, therefore, exclusively controlled by the aggregate breakup and not by any restructuring.

Maximum effective hydrodynamic stress

The relation between the maximum stable aggregate size and the applied maximum effective hydrodynamic stress measured in the nozzle (Figure 4B) was used to recalculate the measured aggregates sizes in the stirred tank reported in Figures 5 and 6. The corresponding maximum hydrodynamic stress values are plotted in Figure 8. When reaching a threshold value, the corresponding stress was under all investigated conditions only a function of Re_{imp}. As the values of hydrodynamic stress are not commonly reported in the mixing community they were recalculated to the corresponding ε_{max} using Eq. 1. The normalized values of ε_{max}/N^3D^2 for nonsparged conditions of up to 150 are in agreement with recent evaluations of the highest values calculated from LES

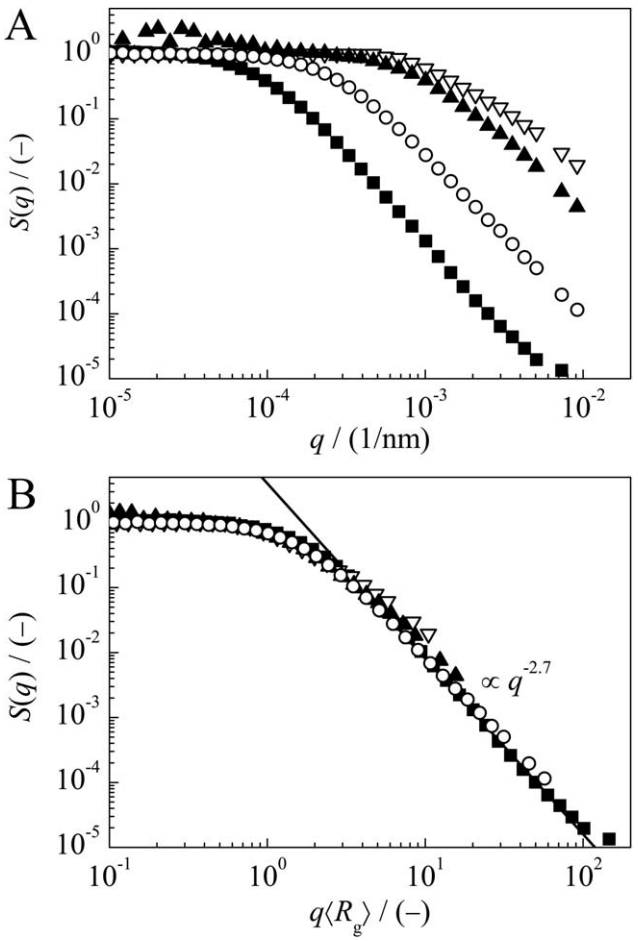

Figure 7. Structure factor, *S(q)*, and fractional dimension, d_f after various breakage conditions.

(A) Steady-state structure factor, *S(q)*, as a function of the scattering amplitude, *q*. Initial aggregates before dilution (closed squares), after dilution (open circles), broken by rising bubbles in the presence (closed up triangles) and absence of surfactant (open down triangles). (B) Evaluation of d_f from the power law of *S(q)* plotted as a function of $q\langle R_g \rangle$. The solid line represents a power law scaling with a slope equal to -2.7.

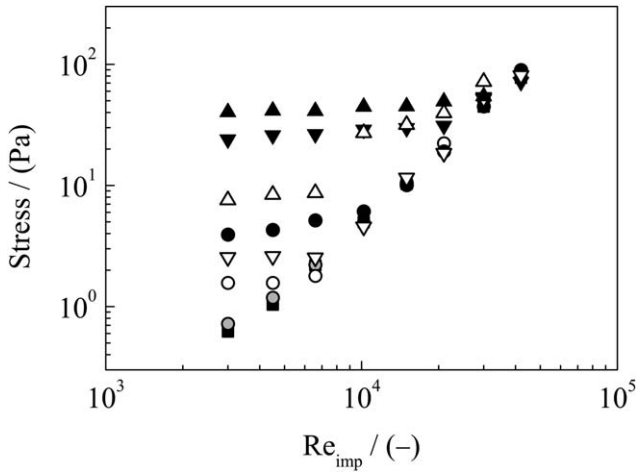

Figure 8. Maximum effective hydrodynamic stress as a function of impeller Reynolds number at various combinations of gas flow rate and nozzle diameter (see Table 2).

by Sungkorn et al.,[65] Micheletti et al.,[66] Soos et al.,[9] and with experimentally determined values of Wichterle et al.[30] using an electrochemical method. Therefore, the maximum effective hydrodynamic stress and also the maximum energy dissipation rate might have been frequently underestimated, in particular regarding laser-based techniques.

In gas–liquid systems, the strongest effect of the gas phase was present at low stirring speeds enabling the identification of different mechanism as a source of the maximum effective hydrodynamic stress. The highest stress values were found when no surfactant was used. Small bubbles of approximately 1.3 mm in diameter broke down the aggregates to submicron sizes even at low gas flow rates (closed up triangles in Figure 8). Conversely, only small maximum stress values were measured for single rising bubbles in surfactant containing solutions, even at high gas flow rates producing large bubbles (closed circles in Figure 8). Furthermore, stress arising from the gas inlet jet varies substantially covering a range from 1 up to 80 Pa (down triangles) as shown in Figure 8.

Figure 9A illustrates the effect of the gas inlet jet on the maximum effective hydrodynamic stress where the stress increases with Re_{jet} above a critical value of 600 according to a power law scaling independent of the applied nozzle size and gas flow rate. Below this critical value, the maximum stress is controlled by bubble rise and, therefore, becomes independent of Re_{jet}. The measured effective stress levels of rising bubbles were found to be dependent on their bubble size. Large bubbles of around 10 mm showed stress values of up to 5 Pa, whereas small bubbles (1.3 mm) formed by the sinter sparger showed only stress values of 0.7 Pa in surfactant containing conditions. This small value coincides well with stress values of 0.3 Pa reported by Koynov et al.[7] calculated for rising bubbles with a diameter of 0.8 mm. In addition, the observed increase of the hydrodynamic stress with bubble diameter is also in agreement with the trend reported by Koynov et al.[7]

The maximum effective stress as a function of bubble diameter in surfactant free solution is presented in Figure 9B. As the stress arising from stirring and the gassing jet could mask the differences of other mechanisms such as bubble burst and bubble rise, the Re_{jet} was set well below 600 and the Re_{imp} was set to 3000. The highest effective stress was caused by small bubbles and its value decreases with increasing bubble size, finally reaching a plateau value of around 10 Pa (Figure 9B). The high τ_{max} values of up to 100 Pa for small bubbles are in good agreement with the calculated values of Boulton-Stone and Blake.[8] In contrast, stresses measured for larger bubbles of several millimeters are one to two orders of magnitude larger compared to those calculated by Boulton-Stone and Blake[8] indicating another source of highest stress. Boulton-Stone and Blake[8] excluded the effect of rising bubbles which could explain the discrepancy for larger bubbles. Given the fact that large rising bubbles resulted in very similar aggregate cluster breakup in surfactant containing and surfactant free conditions, bubble rising becomes the dominant mechanism with increasing bubble diameter.

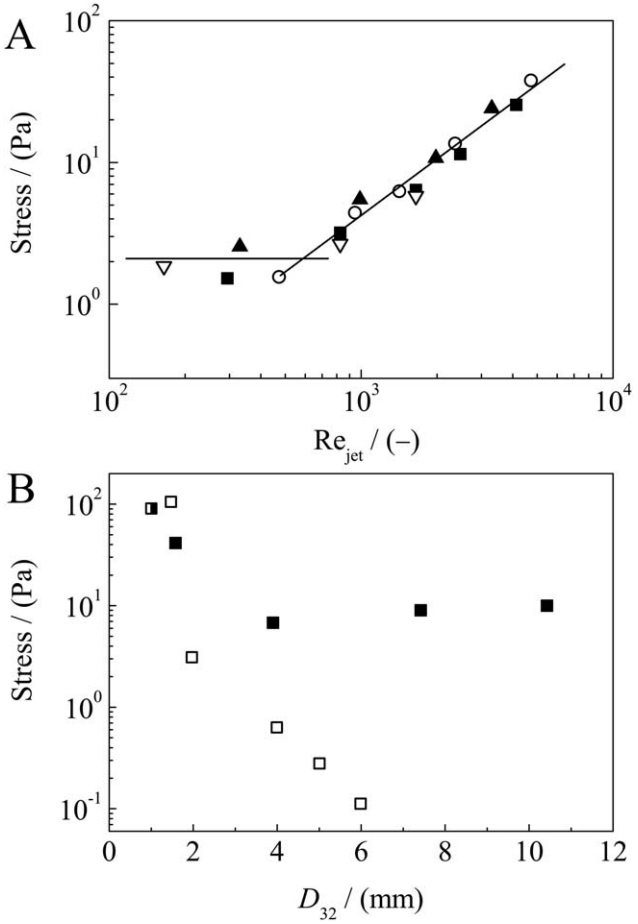

Figure 9. Maximum effective hydrodynamic stress as a function of Re_{jet} and as a function of bubble size.

(A) Maximum effective hydrodynamic stress as a function of Re_{jet} with nozzle diameters of 0.4 mm (closed squares), 0.7 mm (open circles), 1 mm (closed up triangles), and 2 mm (open down triangles) using 0.5 g/L surfactant. (B) Maximum effective hydrodynamic stress as a function of bubble size without surfactant (closed squares). The results of Boulton-Stone and Blake8 considering bubble burst (open squares) are plotted for comparison.

Conclusions

In this work, an aggregate breakup system was applied to experimentally quantify the maximum effective hydrodynamic stress in single and multiphase flow. Knowing the correlation between aggregate size and maximum hydrodynamic stress from well-defined contracting nozzle experiments, the determination of the highest stress values in various systems can be carried out in a time and cost effective way. Although single rising bubbles caused only minor stress values, bubble burst at the gas–liquid interface and the gas inlet jet are possible sources of highest hydrodynamic stress which is in agreement with available data in literature. The employed breakup system overcomes the limitations of previous indirect measurement methods such as resolution, size of the probing particles, single phase restriction, limited operating ranges, and scale-up. Thus, the proposed method is suitable to quantify highest stress values for the development of shear sensitive processes carried out in multiphase flow.

Acknowledgment

The authors would like to thank Jochen Sieck, Benjamin Neunstöcklin, and Daniel Karst for their valuable comments and discussions. This work was financially supported by the SNF Grant 200020_147137/1.

Notation

C = clearance distance, mm
D = impeller diameter, mm
D_{32} = mean Sauter diameter, mm
d_f = fractal dimension
d_{nozzle} = calibration nozzle diameter, mm
d_{jet} = aeration nozzle diameter, mm
H = tank height, mm
$I(0)$ = zero angle intensity
$I(q)$ = angle-dependent intensity
M = torque, Nm
N = rotation speed, s^{-1}
P = power input, m^2/s^3
Po = power number
Q = flow rate, ml/min
q = magnitude of the scattering wave vector, nm
Re_{imp} = impeller Reynolds number
Re_{jet} = aeration jet Reynolds number
Re_{nozzle} = nozzle Reynolds number
$\langle R_g \rangle$ = radius of gyration, μm
$S(q)$ = structure factor
T = tank diameter, mm
V_L = liquid volume, L
V_S = superficial gas velocity, ms^{-1}

Greek letters

ε = energy dissipation rate, m^2/s^3
$\langle \varepsilon \rangle$ = average energy dissipation rate, m^2/s^3
ε_{max} = maximum energy dissipation rate, m^2/s^3
$\langle \varepsilon \rangle_{stirring}$ = energy dissipation rate from stirring, m^2/s^3
ϕ = void fraction
ρ_L = liquid density, kg/m^3
μ_L = dynamic viscosity of the liquid, Pa s
τ = hydrodynamic stress, Pa
$\langle \tau \rangle$ = average hydrodynamic stress, Pa
τ_{max} = maximum effective hydrodynamic stress, Pa

Abbreviations

CARPT = computer-automated radioactive particle tracking computer tomography
CCC = critical coagulation concentration
CFD = computational fluid dynamics
CMD = cluster mass distribution
LDA = laser-doppler anemometry
PIV = particle image velocimetry
PLIF = planar laser induced fluoresence
PEPT = positron emission particle tracking
PMMA = poly(methyl methacrylate)
KPS = potassium persulfate
MMA = methyl methacrylate
RDG = Rayleigh-Debye-Gans
SALS = small angle light scattering
SDS = sodium dodecyl sulphate

Literature Cited

1. Hu W, Berdugo C, Chalmers JJ. The potential of hydrodynamic damage to animal cells of industrial relevance: current understanding. *Cytotechnology*. 2011;63(5):445–460.
2. Nienow AW. Reactor engineering in large scale animal cell culture. *Cytotechnology*. 2006;50(1–3):9–33.
3. Chisti Y. Hydrodynamic damage to animal cells. *Crit Rev Biotechnol*. 2001;21(2):67–110.
4. Chisti Y. Animal-cell damage in sparged bioreactors. *Trends Biotechnol*. 2000;18(10):420–432.
5. Nienow AW, Scott WH, Hewitt CJ, Thomas CR, Lewis G, Amanullah A, Kiss R, Meier SJ. Scale-down studies for assessing the impact of different stress parameters on growth and product quality during animal cell culture. *Chem Eng Res Des*. 2013;91(11): 2265–2274.
6. Zhu Y, Cuenca JV, Zhou W, Varma A. NS0 cell damage by high gas velocity sparging in protein-free and cholesterol-free cultures. *Biotechnol Bioeng*. 2008;101(4):751–760.
7. Koynov A, Tryggvason G, Khinast JG. Characterization of the localized hydrodynamic shear forces and dissolved oxygen distribution in sparged bioreactors. *Biotechnol Bioeng*. 2007;97(2):317–331.
8. Boulton-Stone J, Blake J. Gas bubbles bursting at a free surface. *J Fluid Mech*. 1993;254:437–466.
9. Soos M, Kaufmann R, Winteler R, Kroupa M, Lüthi B. Determination of maximum turbulent energy dissipation rate generated by a rushton impeller through large eddy simulation. *AIChE J*. 2013; 59(10):3642–3658.
10. Baldi S, Ducci A, Yianneskis M. Determination of dissipation rate in stirred vessels through direct measurement of fluctuating velocity gradients. *Chem Eng Technol*. 2004;27(3):275–281.
11. Ducci A, Yianneskis M. Direct determination of energy dissipation in stirred vessels with two-point LDA. *AIChE J*. 2005;51(8):2133–2149.
12. Sharp KV, Adrian RJ. PIV study of small-scale flow structure around a Rushton turbine. *AIChE J*. 2001;47(4):766–778.
13. Escudié R, Liné A. Experimental analysis of hydrodynamics in a radially agitated tank. *AIChE J*. 2003;49(3):585–603.
14. Wernersson E, Trägårdh C. Measurements and analysis of high-intensity turbulent characteristics in a turbine-agitated tank. *Exp Fluids*. 2000;28:532–545.
15. Wernersson E, Trägardh C. Turbulence characteristics in turbine-agitated tanks of different sizes and geometries. *Chem Eng J*. 1999; 72:97–107.
16. Wernersson E, Trägrdh C. Scaling of turbulence characteristics in a turbine-agitated tank in relation to agitation rate. *Chem Eng J*. 1998; 70:37–45.
17. Geng X, Gao Z, Bao Y. PIV Study of flow in an aerated tank with a hollow blade turbine. *Int J Chem React Eng*. 2012;10:A17.
18. Deen NG, Solberg T, Hjertager BH. Flow generated by an aerated Rushton impeller: two-phase PIV experiments and numerical simulations. *Can J Chem Eng*. 2002;80(4):1–15.
19. Montante G, Paglianti A, Magelli F. Experimental analysis and computational modelling of gas–liquid stirred vessels. *Chem Eng Res Des*. 2007;85(5):647–653.
20. Montante G, Laurenzi F, Paglianti A, Magelli F. Two-phase flow and bubble size distribution in air-sparged and surface-aerated vessels stirred by a dual impeller. *Ind Eng Chem Res*. 2010;49(6):2613–2623.
21. Sheng J, Meng H, Fox RO. A large eddy PIV method for turbulence dissipation rate estimation. *Chem Eng Sci*. 2000;55(20):4423–4434.
22. Chiti F, Bakalis S, Bujalski W, Barigou M, Eaglesham A, Nienow AW. Using positron emission particle tracking (PEPT) to study the turbulent flow in a baffled vessel agitated by a Rushton turbine: improving data treatment and validation. *Chem Eng Res Des*. 2011; 89(10):1947–1960.

23. Khopkar AR, Rammohan AR, Ranade VV, Dudukovic MP. Gas–liquid flow generated by a Rushton turbine in stirred vessel: CARPT/CT measurements and CFD simulations. *Chem Eng Sci*. 2005;60(8–9):2215–2229.
24. Devanathan N, Moslemian D, Dudukovic M. Flow mapping in bubble columns using CARPT. *Chem Eng Sci*. 1990;45(8):2285–2291.
25. Dudukovic M. Opaque multiphase flows: experiments and modeling. *Exp Therm Fluid Sci*. 2002;26(6–7):747–761.
26. Kikura H, Murakawa H, Aritomi M. Velocity profile measurements in bubbly flow using multi-wave ultrasound technique. *Chem Eng Commun*. 2009;59(5):1477–1484.
27. Peter CP, Suzuki Y, Büchs J. Hydromechanical stress in shake flasks: correlation for the maximum local energy dissipation rate. *Biotechnol Bioeng*. 2006;93(6):1164–1176.
28. Henzler HJ. Particle stress in bioreactors. *Advances in Biochemical Engineering*, *Vol. 67,* Bayer AG, Wuppertal, Germany. *2000:35–82*.
29. Mahnke EU, Büscher K, Hempel DC. A novel approach for the determination of mechanical stresses in gas-liquid reactors. *Chem Eng Technol*. 2000;23(6):509–513.
30. Wichterle K, Kadlec M, Žák L, Mitschka P. Shear rates on turbine impeller blades. *Chem Eng Commun*. 1984;26(1–3):25–32.
31. Pilz RD, Mahnke EU, Hempel DC. Mechanical stresses in bubble columns and airlift loop-reactors operated in two and three phase modes. *J Chem Eng Jpn*. 2004;37(8):955–961.
32. Pilz RD, Hempel DC. Mechanical stress on suspended particles in two- and three-phase airlift loop reactors and bubble columns. *Chem Eng Sci*. 2005;60(22):6004–6012.
33. Sajjadi S, Yianneskis M. Semibatch emulsion polymerization of methyl methacrylate with a neat monomer feed. *Polym React Eng*. 2003;11(4):715–736.
34. Russel WB, Saville DA, Schowalter WR. *Colloidal Dispersions*. Cambridge: Cambridge University Press, 1989.
35. Moussa AS, Soos M, Sefcik J, Morbidelli M. Effect of solid volume fraction on aggregation and breakage in colloidal suspensions in batch and continuous stirred tanks. *Langmuir*. 2007;23(4):1664–1673.
36. Soos M, Ehrl L, Bäbler MU, Morbidelli M. Aggregate breakup in a contracting nozzle. *Langmuir*. 2010;26(1):10–18.
37. Harshe YM, Lattuada M, Soos M. Experimental and modeling study of breakage and restructuring of open and dense colloidal aggregates. *Langmuir*. 2011;27(10):5739–5752.
38. Harshe YM, Lattuada M. Breakage rate of colloidal aggregates in shear flow through stokesian dynamics. *Langmuir*. 2012;28(1):283–292.
39. Garcia-Briones MA, Brodkey RS, Chalmers JJ. Computer simulations of the rupture of a gas bubble at a gas-liquid interface and its implications in animal cell damage. *Chem Eng Sci*. 1994;49(14):2301–2320.
40. Ma N, Chalmers JJ, Auniņs JG, Zhou W, Xie L. Quantitative studies of cell-bubble interactions and cell damage at different pluronic F-68 and cell concentrations. *Biotechnol Prog*. 2004;20(4):1183–1191.
41. Mollet M, Ma N, Zhao Y, Brodkey R, Taticek R, Chalmers JJ. Bioprocess equipment: characterization of energy dissipation rate and its potential to damage cells. *Biotechnol Prog*. 2004;20(5):1437–1448.
42. Ralston J, Fornasiero D, Hayes R. Bubble–particle attachment and detachment in flotation. *Int J Miner Process*. 1999;56(1–4):133–164.
43. Fan X, Zhang Z, Li G, Rowson N. Attachment of solid particles to air bubbles in surfactant-free aqueous solutions. *Chem Eng Sci*. 2004;59(13):2639–2645.
44. Meier SJ, Hatton TA, Wang DI. Cell death from bursting bubbles: role of cell attachment to rising bubbles in sparged reactors. *Biotechnol Bioeng*. 1999;62(4):468–478.
45. Ehrl L, Soos M, Morbidelli M. Dependence of aggregate strength, structure, and light scattering properties on primary particle size under turbulent conditions in stirred tank. *Langmuir*. 2008;24(7):3070–3081.
46. Soos M, Moussa AS, Ehrl L, Sefcik J, Wu H, Morbidelli M. Effect of shear rate on aggregate size and morphology investigated under turbulent conditions in stirred tank. *J Colloid Interface Sci*. 2008;319(2):577–589.
47. Ehrl L, Soos M, Wu H, Morbidelli M. Effect of flow field heterogeneity in coagulators on aggregate size and structure. *AIChE J*. 2010;56(10):2573–2587.
48. Bäbler MU, Moussa AS, Soos M, Morbidelli M. Structure and kinetics of shear aggregation in turbulent flows. *I. Early stage of aggregation. Langmuir*. 2010;26(16):13142–13152.
49. Blaser S. The hydrodynamical effect of vorticity and strain on the mechanical stability of flocs. PhD Thesis, No. 12851. ETH Zurich, Switzerland, Zurich, 1998.
50. Higashitani K, Iimura K, Sanda H. Simulation of deformation and breakup of large aggregates in flows of viscous fluids. *Chem Eng Sci*. 2001;56:2927–2938.
51. Sonntag RC, Russel WB. Structure and breakup of flocs subjected to fluid stresses. *J Colloid Interface Sci*. 1986;113(2):399–413.
52. Blaser S. Forces on the surface of small ellipsoidal particles immersed in a linear flow field. *Chem Eng Sci*. 2002;57(3):515–526.
53. Blaser S. Flocs in shear and strain flows. *J Colloid Interface Sci*. 2000;225(2):273–284.
54. Blaser S. Break-up of flocs in contraction and swirling flows. *Colloid Surf*. 2000;166(1–3):215–223.
55. Gordillo JM, Sevilla A, Martínez-Bazán C. Bubbling in a co-flow at high Reynolds numbers. *Phys Fluids*. 2007;19(7):077102.
56. Clift R, Grace JR, Weber ME. Bubbles, Drops and Particles, *1st ed*. London: Academic Press Inc., 1978.
57. Choi HM, Kurihara T, Monj H, Matsui G. Measurement of particle/bubble motion and turbulence around it by hybrid PIV. *Flow Meas Instrum*. 2002;12:421–428.
58. Bird R, Stewart W, Lightfoot E. Transport Phenomena. New York: Wiley, 2007.
59. Saha D, Soos M, Lüthi B, Holzner M, Liberzon A, Babler MU, Kinzelbach W. Experimental characterization of breakage rate of colloidal aggregates in axisymmetric extensional flow. *Langmuir*. 2014;30(48):14385–14395.
60. Baldyga J, Podgórska W. Drop break-up in intermittent turbulence: maximum stable and transient sizes of drops. *Can J Chem Eng*. 1998;76(3):456–470.
61. Bäbler MU. A collision efficiency model for flow-induced coagulation of fractal aggregates. *AIChE J*. 2008;54(7):1748–1760.
62. Zaccone A, Soos M, Lattuada M, Wu H, Bäbler MU, Morbidelli M. Breakup of dense colloidal aggregates under hydrodynamic stresses. *Phys Rev E*. 2009;79(6):61401.
63. Paglianti A, Fujasova M, Montante G. A simple model for power consumption in gassed and boiling stirred vessels. *AIChE J*. 2008;54(3):646–656.
64. Trinh K, Garcia-Briones M, Chalmers JJ, Hink F. Quantification of damage to suspended insect cells as a result of bubble rupture. *Biotechnol Bioeng*. 1994;43(1):37–45.
65. Sungkorn R, Derksen J, Khinast J. Euler–Lagrange modeling of a gas–liquid stirred reactor with consideration of bubble breakage and coalescence. *AIChE J*. 2012;58(5):1356–1370.
66. Micheletti M, Baldi S, Yeoh S. On spatial and temporal variations and estimates of energy dissipation in stirred reactors. *Chem Eng Res Des*. 2004;82:1188–1198.

Manuscript received Aug. 18, 2014, and revision received Jan. 16, 2015.